

A hybrid anion exchanger with nanoscale zero valent iron for trace hexavalent chromium removal from drinking water

Annabel Mungan¹, Elizabeth Hjelvik², Anthony Straub^{1,2,3}, and Julie Korak^{1,3*}

¹Department of Civil, Environmental, and Architectural Engineering, University of Colorado

Boulder, Boulder, Colorado

²Materials Science and Engineering Program, University of Colorado Boulder, Boulder,

Colorado

³Environmental Engineering Program, University of Colorado Boulder, Boulder, Colorado

*Corresponding author

Supporting Information

Table of Contents

1 INTRODUCTION	2
1.1 OCCURRENCE AND TOXICOLOGY	2
1.2 ISOTHERM MODELS	2
1.3 SUMMARY OF PREVIOUS WORK	3
2 METHODS	6
2.1 MATERIALS.....	6
2.2 ANALYTICAL METHODS.....	7
2.3 RESIN SYNTHESIS.....	12
2.4 FLUIDIZED BED EXPERIMENTS	12
3 RESULTS AND DISCUSSION	13
3.1 SYNTHESIS TRIALS	13
3.2 RESIN DENSITY CHANGE	25
3.3 BATCH EXPERIMENTS.....	26
3.4 FLUIDIZED BED CALCULATIONS	31
3.5 POST-COLUMN CHARACTERIZATION.....	32
4 REFERENCES	34

1 Introduction

1.1 Occurrence and Toxicology

Chromium occurs in surface and groundwater in two stable oxidation states: trivalent chromium, Cr(III), and hexavalent chromium, Cr(VI).¹ Cr(III), the reduced form, exists as cationic species, exhibiting low solubility and therefore low mobility in soils and water. Common forms of Cr(III) include Cr^{3+} , CrOH^{2+} , $\text{Cr}(\text{OH})_2^+$, and $\text{Cr}(\text{OH})_3(\text{s})$.² Cr(VI), the oxidized form, exists in oxyanion and oxyacid forms and is comparatively more soluble and thus more mobile in water. Its exact species depends upon redox potential, concentration, and pH. Above pH 6.5, which is the range relevant to groundwater, chromate (CrO_4^{2-}) is the prevalent form of Cr(VI).^{2,3} Chromate has a tetrahedral structure, similar to that of sulfate, SO_4^{2-} .²

1.2 Isotherm Models

Empirical Langmuir and Freundlich isotherm models are shown in equations S1-S2.⁴

$$\text{Langmuir: } q_i = \frac{q_{max}K_Lc}{1+K_Lc} \quad (\text{S1})$$

$$\text{Freundlich: } q_i = K_Fc^{\frac{1}{n}} \quad (\text{S2})$$

In these equations, q_i is the resin-phase concentration, c is the equilibrium liquid-phase concentration, and K_L , q_{max} , K_F , and n are empirically fitted constants. **Figure S1** shows these models compared to a linear equation. The Langmuir adsorption model describes a material with the finite number of active sites, with q_{max} equal to the resin capacity. The use of isotherm models is generally discouraged for modeling ion exchange, because it is not constrained by laws of mass action or exchange on a charge equivalent basis.⁵ In this study, Langmuir and Freundlich models are fit as empirical techniques to describe the data and perform a statistical analysis comparing materials.

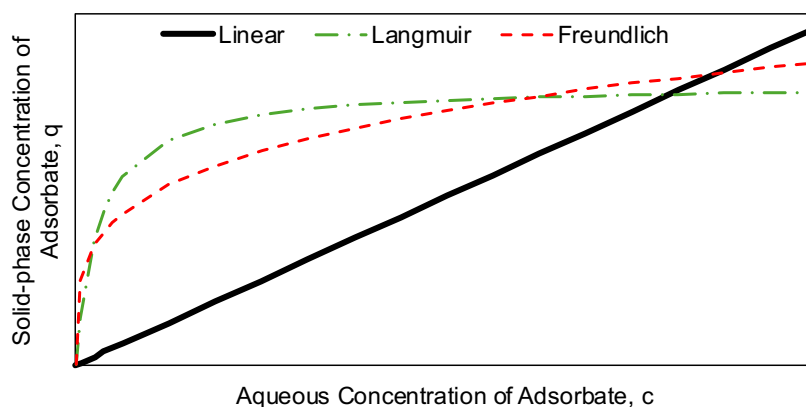


Figure S1. Conceptual representations of Langmuir, Freundlich, and Linear model isotherms.

1.3 Summary of Previous Work

Three studies have investigated NZVI HIX using batch Cr(VI) removal experiments. Fu et al., 2013 synthesized NZVI on a cationic exchange resin, focusing on batch testing for wastewater treatment applications at pH 3-9 with 20-40 mg/L Cr(VI).⁶ NZVI dose, resin dose, pH, and initial concentration of Cr(VI) were all found to be important parameters in batch removal of Cr(VI).⁶ When used resin was re-treated with ferrous iron and borohydride solution, it exhibited 80% removal efficiency in batch tests over 4 reuse cycles for Cr(VI) removal.⁶ Toli et al., 2016 synthesized NZVI on a cationic exchange resin, focusing on batch testing at pH 2.7-8.5 with 5-25 mg/L Cr(VI).⁶ Kinetics were found to follow a first order rate law.⁷ When resin was regenerated using a solution of 2 N HCl, 1 N NaCl, and 1 N NaOH, over 87% Cr(VI) removal efficiency was demonstrated over three cycles.⁷ Gao et al., 2020 synthesized NZVI on a macroporous SBA-IX resin, focusing on batch removal of 20-150 mg/L Cr(VI) from water with pH 3-10 for industrial wastewater treatment applications.⁸ The study reported a resin capacity of 123.14 mg Cr(VI)/g NZVI-impregnated resin using D201, a SBA-IX resin; however, no comparison was made to unmodified ion exchange resin.⁸ The resin was regenerated with 0.1 M NaOH, finding close to 100% Cr(VI) removal efficiency in batch tests over 6 cycles.⁸

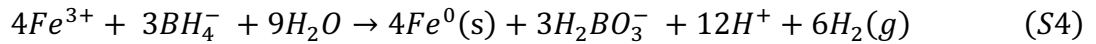
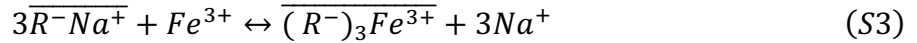
Only a couple studies have performed column experiments for Cr(VI) removal, both using cation exchange resin with NZVI dispersed in it. Toli et al., 2021 synthesized NZVI on a cationic exchange resin, examined column removal of 5 mg/L Cr(VI) from water with pH 4.9.⁹ Running the column to a breakthrough Cr(VI) concentration of 10 µg/L with EBCT of 2.8 minutes found that the column treated less than 10 bed volume (BV) of influent water.⁹ Another study by the same author performed column removal of 0.5-5.2 mg/L Cr(VI) from wastewater effluent with pH 3-7.5. Using an influent water quality of 500 µg/L Cr(VI) and other background constituents including 85 mg/L SO₄²⁻, 347 mg/L Cl⁻, and 192.5 mg/L Na⁺, breakthrough to 100 µg/L Cr(VI) was reached at approximately 300 BV.¹⁰

HIX has been demonstrated at full-scale for arsenic removal and several bench-scale studies have examined hybrid ion exchange for removal of Cr(VI) from wastewater. Relevant Cr(VI) studies and their scope are summarized in **Table S1**. At pH ranges and trace levels of Cr(VI) relevant to drinking water, studies are sparse. In addition, no other studies have yet examined column testing of relevant Cr(VI) concentrations by NZVI-resin using anion exchange resins.

Table S1. Previous studies using NZVI-resin for Cr(VI) removal.

Study	Resin	Experiment	[Cr(VI)] (mg/L)	pH	Application
6	Cationic	Batch	20 – 40	3 – 9	Industrial wastewater treatment
7	Cationic	Batch	5-25	2.7-8.5	Contaminated water
8	Anionic	Batch	20 – 150	3 – 10	Industrial wastewater treatment
9	Cationic	Column	5	4.9	Industrial wastewater treatment
10	Cationic	Column	0.5 – 5.2	2-7.5	Industrial wastewater treatment
Our work	Anionic	Batch Column	175 0.1	8	Groundwater-sourced drinking water treatment

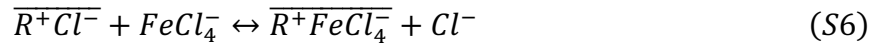
Synthesis of NZVI particles has been studied extensively. The most common approach is through borohydride reduction of ferric or ferrous iron to Fe⁰. Synthesizing NZVI on a cation exchange resin substrate, the technique is more straightforward: Fe³⁺ or Fe²⁺ is exchanged onto the resin (equation S3) and borohydride reaction is performed to reduce the iron (equation S4).



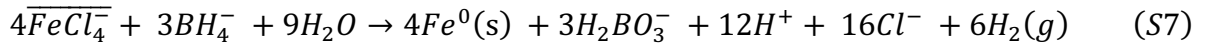
For SBA-IX, exchanging cationic Fe³⁺ onto the positive functional groups is not possible due to the Donnan membrane principle. Therefore, a tetrachloroferrate (FeCl₄⁻) solution must first be created, using FeCl₃•6H₂O and HCl, NaCl, and/or ethanol to convert FeCl₃ into the anionic form.¹¹ In excess-chloride alcohol solutions, FeCl₄⁻ becomes the dominant ferric iron species, according to equation S5.¹²



Next, the FeCl₄⁻ species is exchanged onto the anion exchange resin (equation S6).



The ferric iron is then reduced to Fe⁰, similar to the cation exchange method (equation S7).



This reaction produces solid NZVI, in addition to dihydrogenborate (H₂BO₃⁻), H⁺, Cl⁻, and hydrogen gas (H₂(g)). An illustration of NZVI synthesized on anion exchange resin is shown in **Figure S2**.

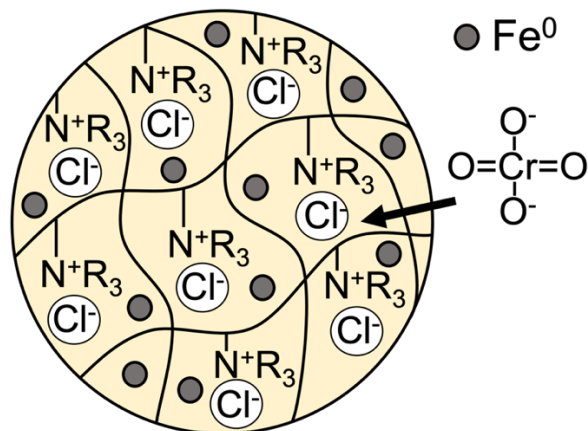


Figure S2. NZVI-impregnated SBA-IX resin for CrO_4^{2-} removal adapted from reference 13.

A handful of prior studies detail their methodologies, shown in **Table S2**, for synthesizing NZVI on strong base anion exchange resin. The majority of the studies began with a $\text{FeCl}_3 \cdot 6\text{H}_2\text{O}$ solution. In order to exchange Fe^{3+} onto the anion exchange resin, the FeCl_3 is converted into FeCl_4^- form using HCl , NaCl , and/or ethanol. One work used 0.5 M FeCl_3 with 1 M HCl , with a resin-to-solution ratio of 1:10 using Purolite A500Plus resin.¹⁴ Another work created a 500 mL solution of 2 M FeCl_3 and 2 M HCl with 10 g of polystyrene anion exchange resin with quaternary ammonium functional groups.¹¹ A third study used an ethanol solution with 0.005 M FeCl_3 and 0.01 M HCl at 70°C for 10 g IRA-402 resin.¹⁵ A fourth work used 100 mL of solution of 1 M HCl with 10% ethanol, ample NaCl , and 1 M FeCl_3 to exchange onto 1 g macroporous polystyrene anion exchange resin.¹⁶

Two other studies proposed different methods for impregnating iron on SBA-IX resin. Tai et al., 2016 used a 40 mL solution of $\text{FeCl}_2 \cdot 4\text{H}_2\text{O}$ to stir 5 g anion exchange resin, according to their procedure to exchange Fe^{2+} .¹⁷ It is uncertain how effectively the Fe^{2+} entered their anion exchange resin, however, due to the Donnan membrane principle. Gao et al., 2020 used a 100 mL solution with 0.09 M FeCl_3 to stir 1 g D201 resin, without mention of how Fe^{3+} was exchanged onto the anion exchange resin.⁸

After stir times ranging from 30 minutes-12 hours^{8,15}, procedures included generic rinsing of FeCl_4^- -resin¹⁴, 5 times rinsing in alcohol¹¹, and rinsing with DI water until filtrate pH 7 was reached¹⁵.

Next, either NaBH_4 or KBH_4 were used as reducing agents for the iron, ranging from 2 M¹⁴, ultrasonic shaking in 1% NaBH_4 ¹¹, varying NaBH_4 or KBH_4 concentration from 0.9-7.2%^{16,18,19}, titration of 20 mL 10% (m/v) KBH_4 ¹⁷, and titration of 100 mL 0.36 M NaBH_4 ⁸.

After reduction, common treatments included centrifugation⁸, resin rinsing¹⁷ with deoxygenated water^{11,14} or absolute ethanol^{8,14,19}, vacuum drying^{8,11,14}, or drying at room temperature¹⁵.

Table S2. Prior methodology for NZVI synthesis on SBA-IX resin.

Study	Resin mass (g)	Fe (M)	Addition to convert to FeCl ₄ ⁻	Fe stir (h)	Fe rinse solution	BH ₄ ⁻ (M)	NZVI Rinse	Drying	Other
14	–	0.5	1 M HCl	4	–	2	DI water and alcohol	Vacuum at 30°C	–
11	10	2	2 M HCl	10	Alcohol	0.26	Deoxy water	Vacuum	Ultrasonic shaking in BH ₄ ⁻
17	5	0.25	–	2	DI water	1.9	DI water	–	Used Fe ²⁺ , BH ₄ ⁻ titrated
8	1	0.089	–	0.5	–	0.36	Absolute ethanol	Vacuum	BH ₄ ⁻ titrated, Centrifuged
19	1	–	HCl	4	Absolute ethanol	0.17 - 1.3	Ethanol	Vacuum at 40°C	–
15	10	0.005	0.01 M HCl in ethanol at 70°C	12	DI water until pH = 7	0.02	NaCl soak	Room temp for 48 h	–
16	1	1	1 M HCl NaCl 10% ethanol	4	–	1.3	NaCl, NaOH, HCl, and ethanol	45°C	–
Our work	10	0.05	0.1 M HCl in ethanol at 70°C	12	Absolute ethanol	0.1	Absolute ethanol	Vacuum	BH ₄ ⁻ stir at 50°C

2 Methods

2.1 Materials

All chemicals were analytical reagent grade. Solids used included ferric chloride (FeCl₃•6H₂O), sodium borohydride (NaBH₄), 1,5-diphenylcarbazine (C₁₃H₁₄N₄O), sodium sulfate (Na₂SO₄), sodium chloride (NaCl), sodium nitrate (NaNO₃), and sodium bicarbonate (NaHCO₃). Solutions used included absolute ethanol (C₂H₆O), acetone, hydrochloric acid (HCl), sulfuric acid (H₂SO₄), nitric acid (HNO₃), 1000 mg/L sodium chromate (Na₂CrO₄), and 5% w/v sodium chromate tetrahydrate (Na₂CrO₄•4H₂O). N₂ gas was used for deoxygenating solutions. Ultrapure type 1 water (Milli-Q®) was used for all experiments, except for column experiments, which used type 2 water (ion exchange and granular activated carbon treated) for influent water. Alconox Citranox® was used to clean plasticware and Liquinox® was used to clean glassware, followed by rinsing with ultrapure type 1 Milli-Q® water.

Purolite® A600E, A500Plus, and S106 resins and LANXESS Lewatit® TP 107 resin were selected as NZVI synthesis substrates. These four resins were chosen based on their variety of resin properties shown in **Table S3**, including strong base, weak base, gel, macroporous, polystyrene, and polyacrylate. A600E, TP 107, and S106 resins are used specifically for Cr(VI) treatment, with both A600E and TP 107 tested in pilot- and field-scale applications^{20,21}. A500Plus

is typically used for demineralization and removal of silica²². After initial synthesis experiments, A600E was selected as the primary resin for batch and column testing.

Table S3. Properties of selected resins as reported by manufacturers.

Resin	A600E	A500Plus	TP 107	S106
Manufacturer	Purolite®	Purolite®	LANXESS Lewatit®	Purolite®
Strong or Weak Base	SBA	SBA	SBA	WBA
Gel or Macroporous	Gel	Macro	Macro	Macro
Matrix	Polystyrene	Polystyrene	Polyacrylate (acrylic)	Epoxy Polyamine
Functional Group	Type I Quaternary Ammonium	Type I Quaternary Ammonium	Quaternary Ammonium	Polyamine
Ionic Form	Chloride	Chloride	Chloride	Free Amine
Manufacturer Reported Capacity (eq/L)	1.6	1.15	2.4	2
Particle Size Range (µm)	570 ± 50	300 - 1200	450 - 650	300 - 2000

2.2 Analytical Methods

Inductively coupled plasma mass spectrometry (ICP-MS) was used to quantify total chromium and iron concentrations, using an EPA 6020B method with collision cell gases (helium or hydrogen) to decrease molecular ion interferences. All samples analyzed by ICP-MS were diluted to between 5 and 500 µg/L as Cr and acidified to 1% HNO₃ with trace metal grade acid. Ion Chromatography (IC) was used to quantify sulfate, chloride, and nitrate concentrations, using the EPA 300.1 method. Analysis used an AS18-Fast-4µm (Dionex IonPac) column and potassium hydroxide eluent. Analytes were detected using either suppressed conductivity or absorbance at 215 nm. For ICP-MS and IC, quality control included daily calibration, independent calibration verification, spectral interference checks (ICP-MS only), sample replicates, and matrix spikes.

The pH of samples was determined using a Mettler Toledo InLab® Expert Go-ISM pH sensor, calibrated daily with pH 4, 7, and 10 buffer solutions. Electrical conductivity was determined using a Mettler Toledo InLab® 710 conductivity sensor, calibrated daily with a 1413 µS/cm standard solution.

For preliminary screening experiments, a variety of colorimetric methods were used to measure Cr(VI) and iron concentrations, using a Hach DR6000 UV-VIS Spectrophotometer. For concentrations from 1.95 µg/L to 250 µg/L Cr(VI), a modified EPA 7196A method was developed to minimize sample volume and hazardous Cr(VI) waste based on the Standard Method for the Examination of Water and Wastewater 3500-Cr D and Lace et al., 2019²³. The method reacts Cr(VI) with 1,5-diphenylcarbazide (DPC) in acidic conditions to form a pink-colored complex that absorbs at 540 nm. First, an acetone solution of 0.4 M H₂SO₄ with 0.5% 1,5-diphenylcarbazide was created. Then, 2 mL of this solution was added to 10 mL of sample. Absorbance was measured on the spectrophotometer at 540 nm using a 50 mm, semi-micro quartz cuvette that held 5 mL of

sample. Each day sampling occurred, a fresh DPC solution was created, as the solution became discolored after several hours. The 50 mm path length was selected to increase absorbance values, as following the Beer-Lambert Law (equation S8)

$$A = cl\varepsilon(\lambda) \quad (\text{S8})$$

Where A is absorbance, c is concentration of sample (mol/L), l is the light pathlength (cm), and ε is the molar absorptivity of the solution (L/mol-cm) as a function of wavelength, λ . Thus, by increasing pathlength, absorbance readings increased to a measurable range from 0.01 to 0.9. A calibration curve, shown in **Figure S3**, was made using a 1000 $\mu\text{g/L}$ Cr(VI) stock to create standards from 1.95 $\mu\text{g/L}$ to 250 $\mu\text{g/L}$ Cr(VI).

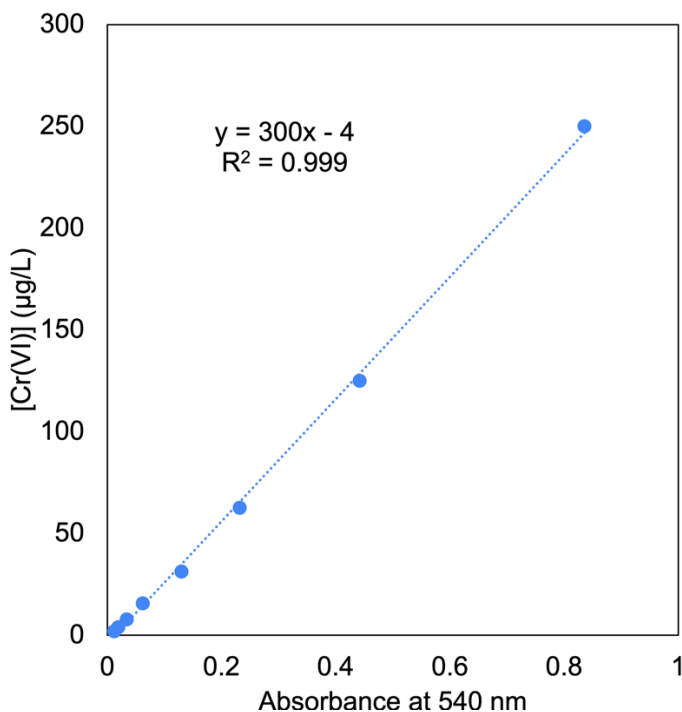


Figure S3. 1,5-Diphenylcarbazide method calibration curve for measuring Cr(VI) concentrations in water with a 50 mm path length.

For concentrations from 195 $\mu\text{g/L}$ to 25 mg/L, Cr(VI) samples were measured directly at 373 nm using a 10 mm pathlength, using the absorbance of chromate at this wavelength.^{24,25} The calibration curve is shown in **Figure S4**, which was made using a 1000 mg/L Cr(VI) stock to create a standard curve. All samples with Cr(VI) above 25 mg/L were diluted before absorbance was measured.

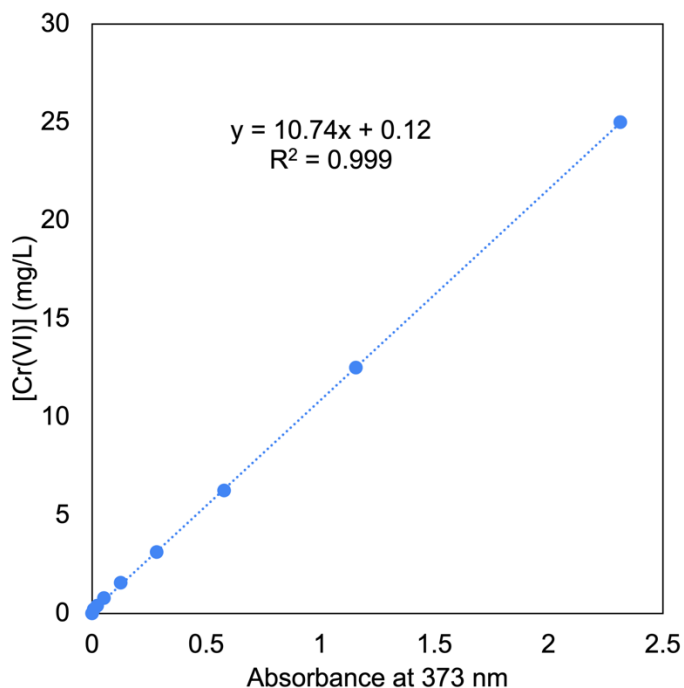


Figure S4. Calibration curve for measuring Cr(VI) concentrations in water.

To measure concentrations of iron in preliminary experiments, Fe^{3+} was also measured by a colorimetric method. All iron samples were diluted in a 0.2 M HCl absolute ethanol solution. In this high chloride-ethanol solution, FeCl_4^- becomes the dominant iron species, with absorbance peaks shown in **Figure S5**.¹²

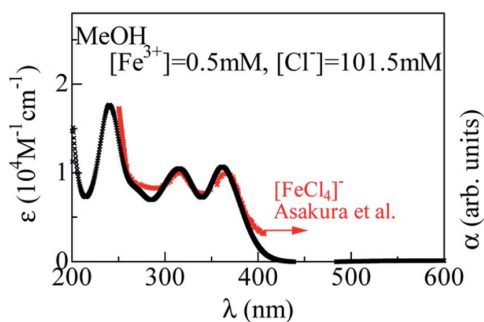


Figure S5. Molar absorptivity of FeCl_4^- in an excess-chloride methanol solution. Reproduced from reference 12 with permission from the Royal Society of Chemistry.

To validate this method, ferric chloride (FeCl_3) was used to create standards with Fe^{3+} concentrations of 50 $\mu\text{g/L}$ to 25 mg/L in 0.2 M HCl in ethanol solution. The following peaks, shown in **Figure S6**, were found by performing a full UV-VIS scan.



Figure S6. Full scan of 5.5 mg/L Fe^{3+} in an excess-chloride ethanol solution.

Thus, a calibration curve, shown in **Figure S7**, based on known iron concentrations was created and measured at 362 nm using a 10 mm path length. Iron samples were diluted with 0.2 M HCl in ethanol solution to fall within the calibration range.

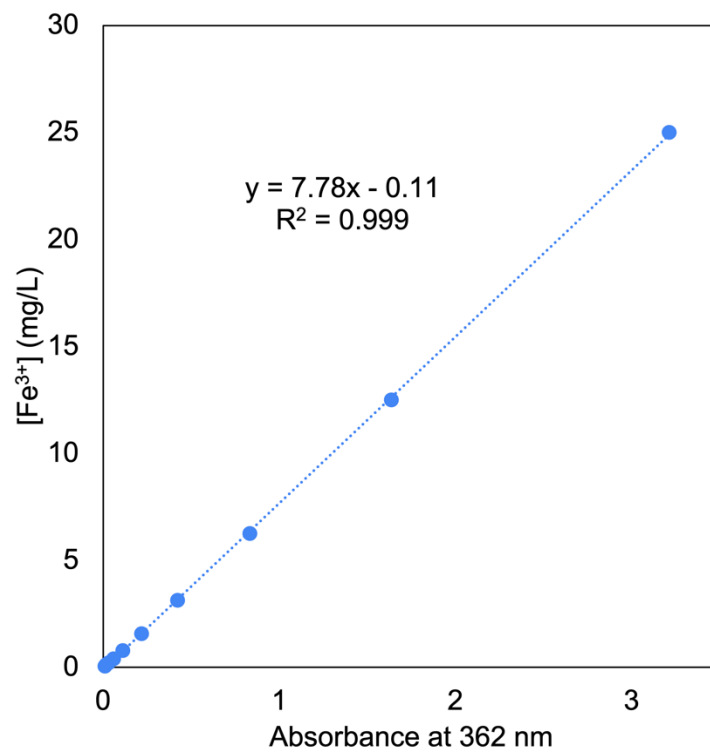
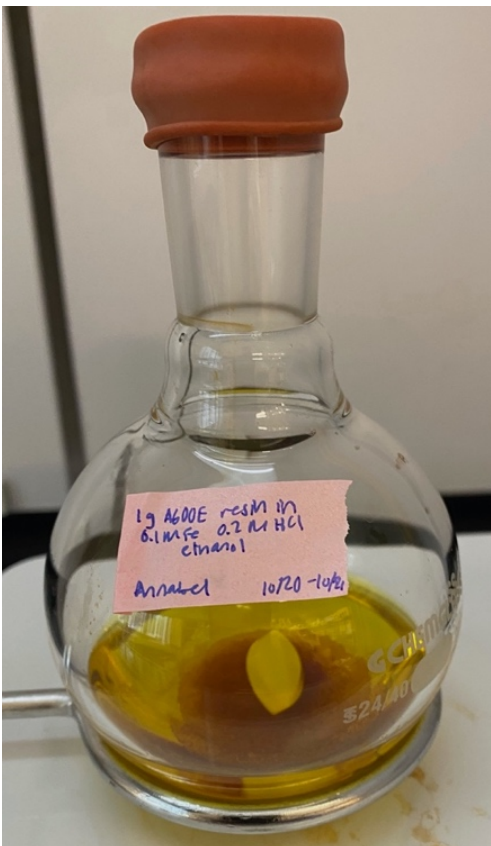


Figure S7. Calibration curve of Fe³⁺ in an excess-chloride ethanol solution at 362 nm.

2.3 Resin Synthesis

Figure S8 shows photos of the experimental set-up for synthesis of two batch sizes. A round bottom flask was used to synthesize batches of 1 gram of resin. A beaker was used to scale-up synthesis to 20 grams of resin.

A)



B)

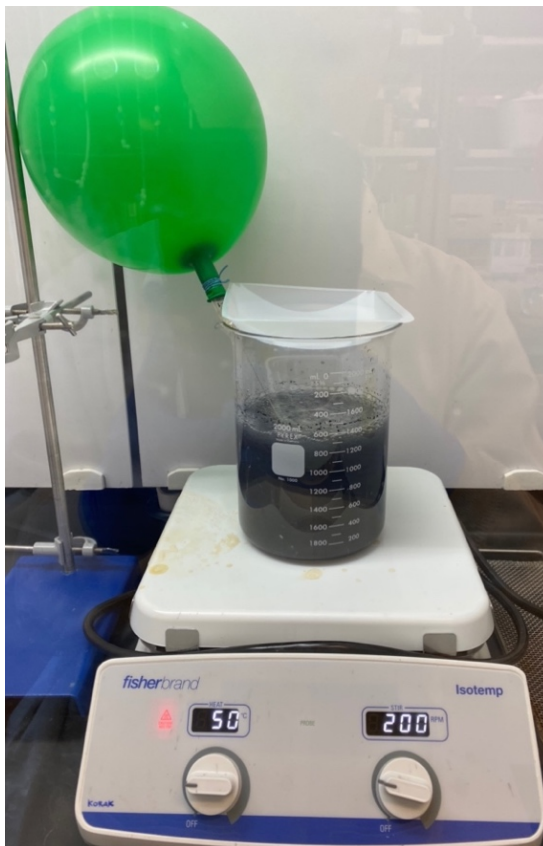


Figure S8. Photos of experimental set-up during resin synthesis A) Step 1: FeCl_4^- exchange onto A600E resin, and B) Step 2: Reduction of Fe^{3+} to Fe^0 by NaBH_4 for A600E resin.

2.4 Fluidized Bed Experiments

In order to perform the column experiment, a laboratory setup was first configured with influent water passing from a 25-gallon barrel by a Masterflex[®] L/S[®] pump upflow through the column and into an effluent water composite waste bin. Pressure gauges were placed before and after the column to measure pressure drop in the system. 18 mL of wet A600E or NZVI-A600E resin was placed into the column with Fluval[®] FX5 polyester pad placed in the top and bottom of the column to prevent resin loss. After resin was loaded, the column was backwashed with type 2 water to remove air bubbles from the system. Next, 5 BV (90 mL) of 2 N NaCl was passed upflow through the column to ensure all Cl^- was exchanged on all ion exchange sites. Following this

regeneration, type 2 water was sent through the column until the effluent conductivity was below 200 $\mu\text{S}/\text{cm}$. The upflow fluidized bed column setup is shown in **Figure S9**.

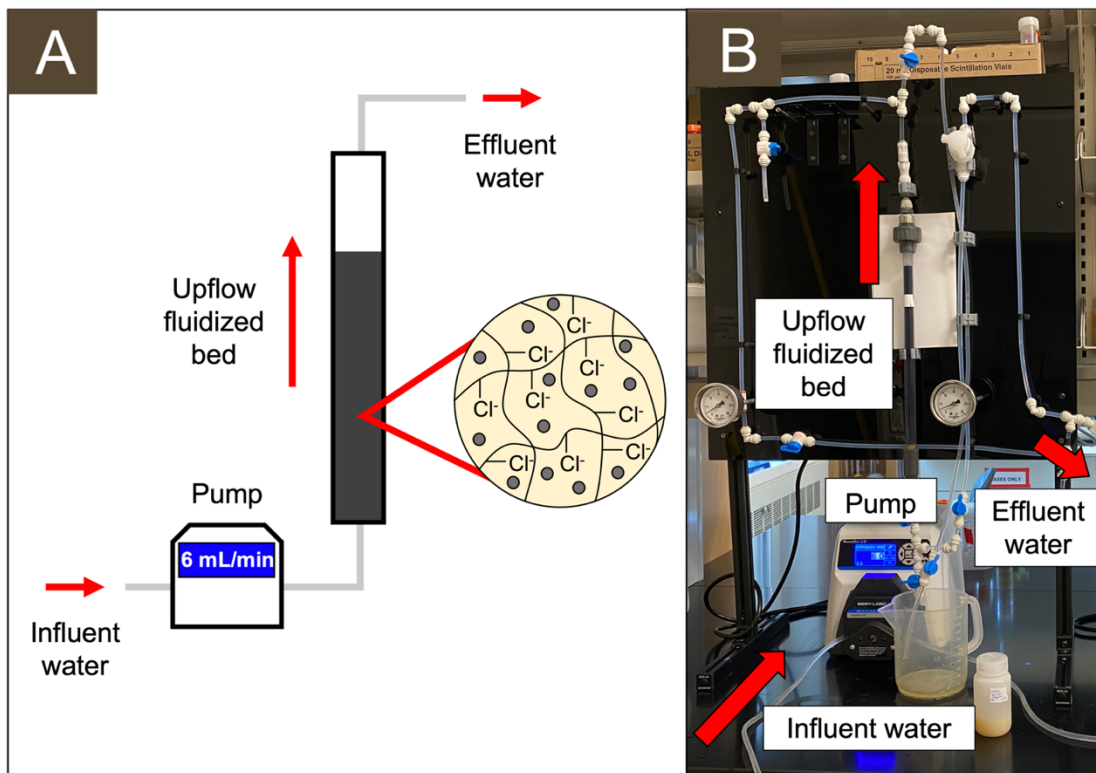


Figure S9. (A) Schematic and (B) photo of upflow fluidized bed column setup.

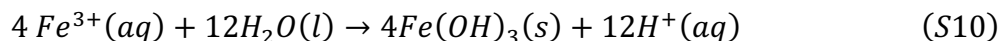
During loading, an effluent sample was taken every 200 BV until 10 $\mu\text{g}/\text{L}$ Cr(VI) breakthrough was reached, according to the anticipated Cr(VI) MCL in the State of California. Composite effluent water was also collected in a tub and weighed every 400 BV to ensure volumetric flow rate was maintained.

3 Results and Discussion

3.1 Synthesis Trials

To load FeCl_4^- on the resin, absolute ethanol was required and could not be diluted, and excess HCl at twice the molar concentration of iron was required. A temperature of 70°C encouraged exchange of FeCl_4^- onto the resin, as opposed to room temperature. A visual indicator of successful resin loading with FeCl_4^- was a bright orange color.

To prepare the FeCl_4^- -resin for the reduction reaction, rinsing 5x in absolute ethanol was best for removal of impurities and excess iron. Deionized (DI) water was not used for rinsing to prevent formation of $\text{Fe}(\text{OH})_3(\text{s})$ on the resin, according to equations S9-S10.

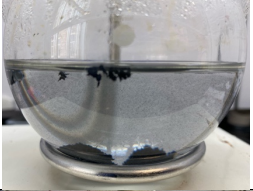
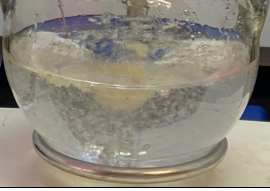

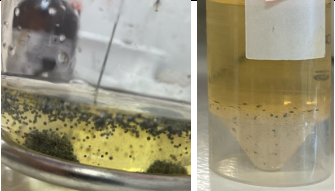
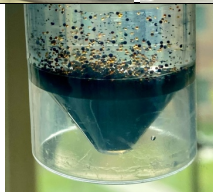





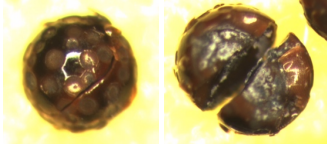
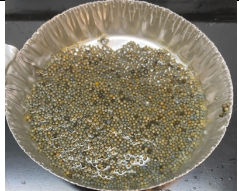
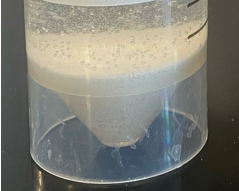

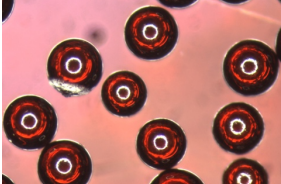
While exchange of BH_4^- onto the resin and reduction of titrated FeCl_3 was possible, the reaction was not stable and had the potential of reversing itself, as shown in experiment 5 in **Table S4**. The best method of NaBH_4 addition was to first air dry the FeCl_4^- -resin for 24 h prior to the NaBH_4 reaction to prevent aggregate iron from forming in solution. A $\text{N}_2(\text{g})$ -purged NaBH_4 solution was created and the dry FeCl_4^- -resin was introduced directly into the solution. Titration of NaBH_4 solution into DI water with the FeCl_4^- -resin led to hydrolysis of the pre-loaded FeCl_4^- . Titrating NaBH_4 into DI water caused a reaction between NaBH_4 and Fe^{3+} in solution rather than on the resin, as shown in experiments 18, 19, and 22 in **Table S4**. The reaction was performed on a hot plate set at 50°C to increase the reaction rate. The reaction was substantially complete after 15 minutes as indicated by reduced bubbling. A mass of 10 g FeCl_4^- -resin was determined to be the maximum amount of resin that could be reduced in one 2000 mL beaker with 1200 mL of solution.


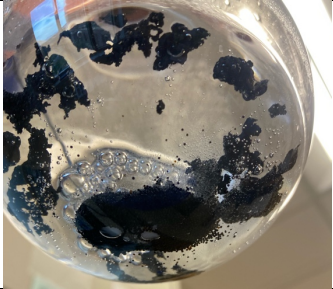


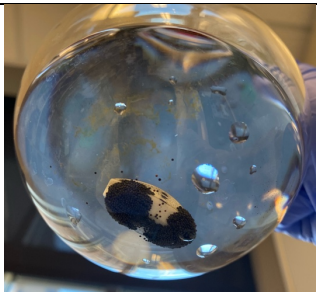
After the reduction reaction was complete, selection of rinse solution was also important. The most successful approach rinsed NZVI-resin with absolute ethanol and deoxygenated DI water. Rinsing with either oxygenated DI water or HCl oxidized the iron on the resin more quickly as indicated by a color change from black to red. The resin was dried in a vacuum desiccator for 24 h to prevent oxidation by $\text{O}_2(\text{g})$.


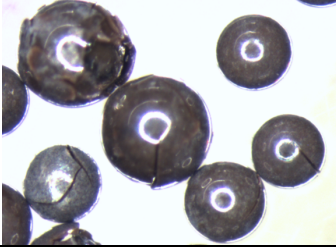


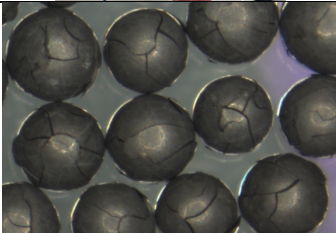
Of the four resins tested (i.e., A600E, TP 107, A500Plus, and S106), A600E and TP 107 produced the best NZVI-resin products based on upon initial screening, as exemplified in experiments 23 and 28. A500Plus and S106, on the other hand, did not turn completely black nor magnetic during experiments, as shown in experiments 14, 15, and 27. Because A600E is a common resin for $\text{Cr}(\text{VI})$ treatment, this resin was selected for further synthesis optimization and characterization through batch and column testing. Synthesis optimization, characterization, and performance testing of NZVI immobilized on TP 107, A500Plus, and S106 resins is suggested for future work.

Table S4. Synthesis of NZVI screening experiments using anion exchange resin, with each row documenting the incremental change in approach.

Experiment	Approach	Outcome	Images
1	Stirred A600E resin in FeCl ₃ solution for 0.5 h, titrated NaBH ₄ directly into FeCl ₃ solution	NaBH ₄ reacted with aqueous Fe ³⁺ instead of resin and could not be separated out from aqueous NZVI.	
2	Drained FeCl ₃ solution after 0.5 h stir, rinsed resin 3x with water, titrated NaBH ₄ onto resin	Resin floated in NaBH ₄ but did not react, which shows that SBA-IX resin cannot exchange Fe ³⁺ directly.	
3	Stirred for 16 h in FeCl ₃ solution	No reaction again, since SBA-IX resin cannot exchange Fe ³⁺ directly.	—
4	Used FeSO ₄ solution instead of FeCl ₃ solution	SBA-IX resin cannot exchange Fe ²⁺ directly either.	
5	Soaked resin in NaBH ₄ and then titrated in FeCl ₃	Resin initially turned a grey-black and was magnetic after titration of FeCl ₃ , but the reaction reversed within 0.5 h, turning the resin white.	
6	Stirred resin in 0.2 M FeCl ₃ with 0.4 M HCl in ethanol (FeCl ₄ ⁻ solution)	Resin turned partially magnetic black, indicating formation of NZVI, but also partially orange-red.	
7	Pre-soaked resin in Cl ⁻ prior to stir in FeCl ₄ ⁻ solution	Same result as experiment 6 indicates that Cl ⁻ pre-soak was not important.	
8	Soaked resin in NaBH ₄ and then titrated in FeCl ₃ , this time removing resin from reaction after 5 minutes before the reaction could reverse	Resin turned a grey-black color, but was not deep black. NaBH ₄ -first method was terminated.	

Experiment	Approach	Outcome	Images
10	Stirred resin in FeCl_4^- solution at 70°C , rinsed FeCl_4^- resin in 2.5 L DI water until $\text{pH} = 6$	FeCl_4^- resin turned deep red due to formation of $\text{Fe}(\text{OH})_3(\text{s})$. Resin remained predominantly red after NaBH_4 reduction.	
11	Decreased concentration to 0.005 M FeCl_3 and 0.01 M HCl in ethanol and reduced with 0.02 M NaBH_4	No reaction occurred.	—
12	Increased concentration to 1 M FeCl_3 and 2 M HCl in ethanol and reduced with 4 M NaBH_4	Using a dissecting microscope, resin cracked and had red-brown color with white crystals, which may be excess NaBH_4 on the resin.	
13	Used TP 107 resin	Resin appeared to react with NaBH_4 , but upon closer inspection was yellow-grey.	
14	Used A500Plus resin	Resin decomposed into a powder after the FeCl_4^- loading step. No reaction with the NaBH_4 occurred.	
15	Used S106 resin	Resin appeared to react with NaBH_4 . Upon closer inspection, resin was dark red. Future tests focus on A600E.	
16	Stirred A600E resin in FeCl_4^- solution at 70°C , rinsed FeCl_4^- resin in NaHCO_3 until $\text{pH} = 8.3$	FeCl_4^- resin turned deep red due to formation of $\text{Fe}(\text{OH})_3(\text{s})$. Resin remained deep red after reaction with NaBH_4 .	

Experiment	Approach	Outcome	Images
17	Rinsed FeCl_4^- resin in NaOH until pH = 8.3, dissolved NaBH_4 titration solution in absolute ethanol instead of DI water, and performed NaBH_4 reduction in ice bath	FeCl_4^- resin turned deep red due to formation of $\text{Fe}(\text{OH})_3(\text{s})$.	
18	Rinsed FeCl_4^- resin 1x with absolute ethanol instead of DI water, performed reduction reaction at 70°C	Since the DI water rinsing appeared to cause $\text{Fe}(\text{OH})_3(\text{s})$ formation, rinsing with ethanol formed black, magnetic resin. However, NZVI also formed in the bulk solution and stuck to the resin.	
19	Scaled up from 1 g resin to 10 g and rinsed FeCl_4^- resin 5x with absolute ethanol, tried to separate aggregate NZVI from resin in sieve	Separation of bulk aggregated NZVI from resin using sieve was unsuccessful.	
20	To reduce ethanol use, stirred resin in 0.1 M FeCl_3 0.2 M HCl in 20% ethanol instead of absolute ethanol	Absolute ethanol was found to be important to exchange FeCl_4^- onto the resin (see image of FeCl_4^- resin stirred in absolute ethanol on left compared to 20% ethanol on right).	
21	Rinsed 0.5 g FeCl_4^- resin 11x with absolute ethanol	Black magnetic NZVI formed on the resin and no aggregate formed, however an excessive amount of absolute ethanol was used to achieve this result which is not practical for upscaling.	
22	Rinsed 20 g FeCl_4^- resin 10x with absolute ethanol	Black magnetic NZVI formed on the resin but aggregate NZVI also formed in solution and stuck to the resin as in experiments 18-19.	—

Experiment	Approach	Outcome	Images
23	Rinsed 4 g FeCl_4^- resin 5x with absolute ethanol and then air dried for 24 h, then added dried FeCl_4^- resin directly into NaBH_4 solution	Black magnetic NZVI formed on the resin and no aggregate formed. However, dissecting microscopy revealed resin had small cracks and NZVI-resin bubbled when placed in DI water.	 
24	Soaked NZVI-A600E in 0.005 M HCl to attempt to quench bubbling	HCl soak caused NZVI-resin to oxidize quickly, turning a yellow-brown color.	
25	Performed reduction reaction at 25°C	No visual differences from 70°C.	—
26	Performed reduction reaction at 50°C	No visual differences from 70°C, so moved forward with reaction at 50°C.	—
27	Used conditions that were optimized for A600E on A500Plus resin	While A500Plus did not decompose like in experiment 14 this time, resin was yellow and grey instead of black.	
28	Used conditions that were optimized for A600E on TP 107 resin	Black magnetic NZVI formed on the resin and no aggregate formed. However, dissecting microscopy revealed resin was cracked, and NZVI-resin bubbled when placed in DI water.	

Reduction by NaBH_4 was tested systematically using a central-composite design. Gas production was observed from all nine NaBH_4 concentration and volume conditions, as shown in **Figure S10**. Differences in resin visual appearance and cracking is documented in **Table S5**.

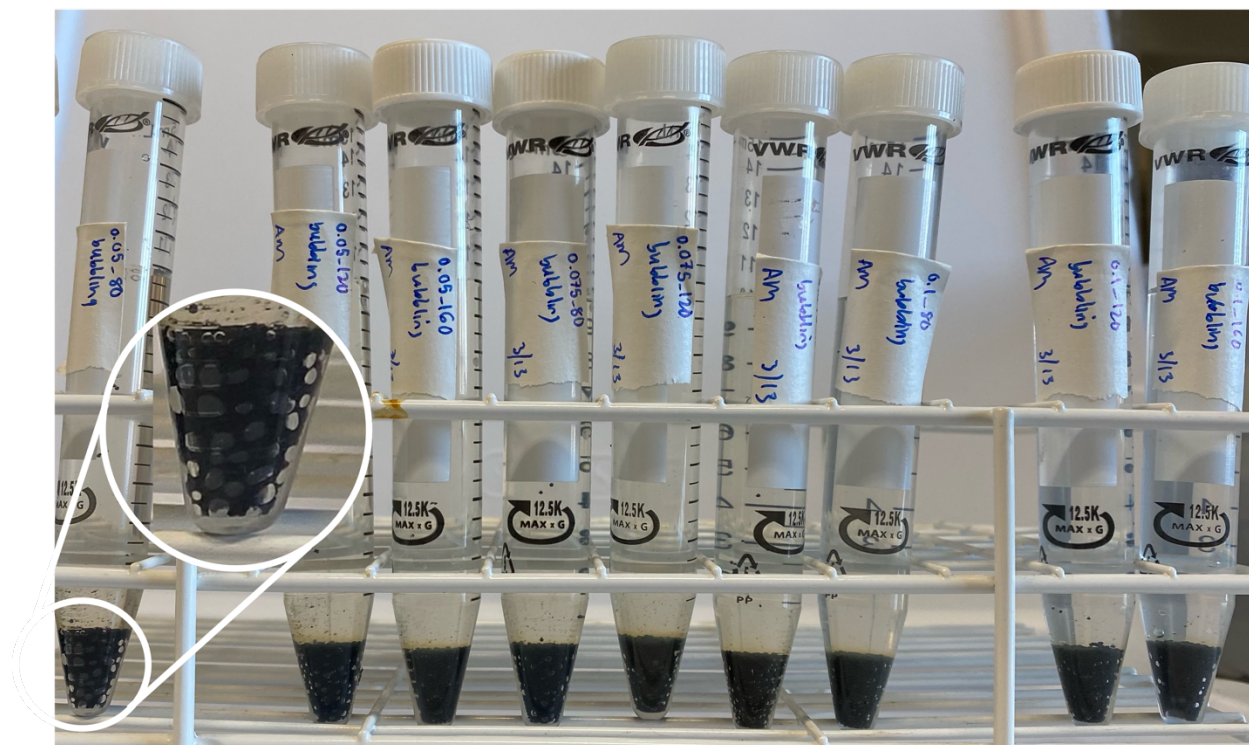
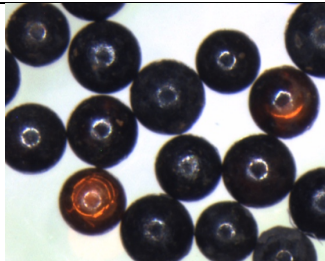
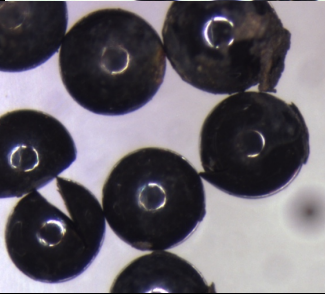


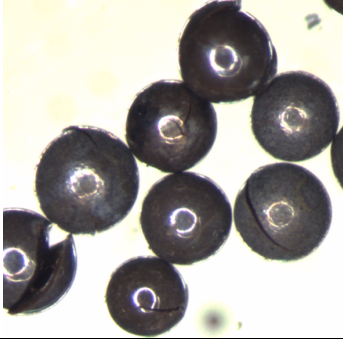
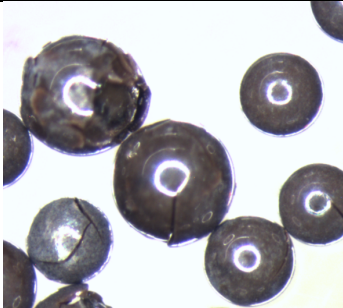
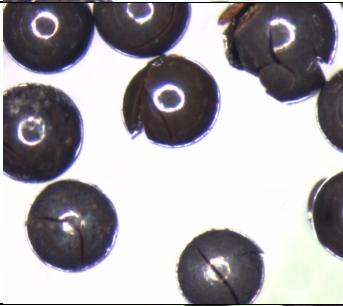
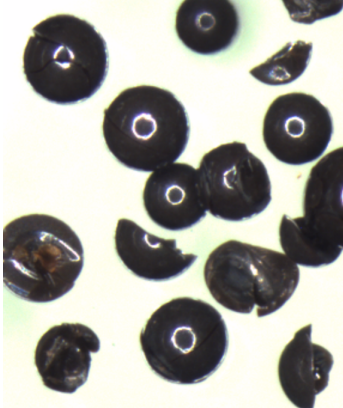
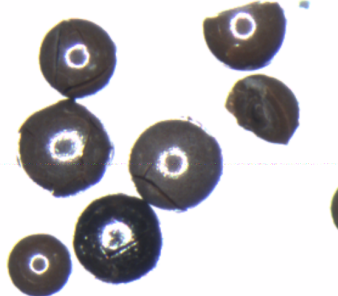


Figure S10. NZVI-A600E produced gas bubbles at all 9 conditions tested.

Table S5. Dissecting microscopy images of NZVI-A600E over varied NaBH₄ conditions.

[NaBH ₄] (M)	NaBH ₄ volume (mL)	[NaBH ₄]/ [FeCl ₄] (mol/mol)	Resin cracked (%)	Results and discussion	Dissecting microscope image
0.05	80	2.7	1	While no resin was cracked, some resin beads remained in FeCl ₄ ⁻ and had not been reduced.	
0.05	120	4.1	16	Some resin were cracked and some aggregate NZVI was oxidizing on the resin.	
0.05	160	5.5	19	Some resin were cracked and some aggregate NZVI was oxidizing on the resin.	
0.075	80	4.1	42	Resin beads were chipped slightly.	

[NaBH ₄] (M)	NaBH ₄ volume (mL)	[NaBH ₄]/ [FeCl ₄] (mol/mol)	Resin cracked (%)	Results and discussion	Dissecting microscope image
0.075	120	6.1	63	Resin beads were chipped slightly.	
0.075	160	8.2	67	Resin beads were chipped slightly.	
0.1	80	5.5	58	Resin beads were chipped slightly.	
0.1	120	8.2	89	Many resin beads were broken into pieces.	

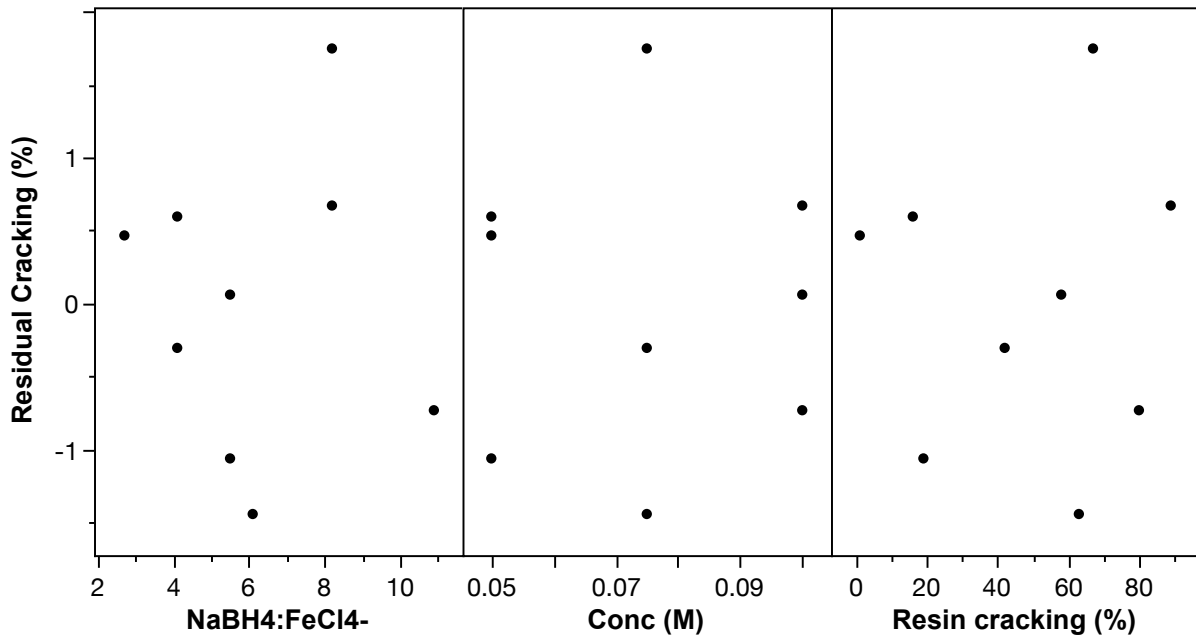
[NaBH₄] (M)	NaBH₄ volume (mL)	[NaBH₄]/ [FeCl₄] (mol/mol)	Resin cracked (%)	Results and discussion	Dissecting microscope image
0.1	160	10.9	80	Many resin beads were broken into pieces.	

A response surface model was fit to explain the dependence of resin cracking on the experimental conditions for iron reduction. Starting with resin loaded with the same resin-phase iron concentration, different combinations of sodium borohydride (NaBH₄) and the ratio of NaBH₄ to resin-phase iron were tested following a central composite design. **Table S6** reports the ANOVA analysis demonstrating term significance. Residual plots are shown in **Figure S11** to demonstrate model adequacy. **Figure S11a** shows that residuals appear random and centered around zero with respect to each explanatory variable and model predictions. **Figure S11b** shows that the residuals are normally distributed.

Table S6. ANOVA analysis of response surface model for dependence of cracking (%) upon both sodium borohydride concentration ([NaBH₄]) and ratio of NaBH₄ to resin-phase iron.

Source	Degrees of Freedom	Sum of Squares	Mean Square	F Ratio	P value
Model	5	7492	1498	568	0.0001
[NaBH ₄]	1	1448	1448	549	0.0002
Ratio (NaBH ₄ :FeCl ₄ ⁻)	1	657	657	249	0.0006
Ratio*Ratio	1	337	337	128	0.0015
[NaBH ₄]*[NaBH ₄]	1	400	400	152	0.0012
[NaBH ₄]*Ratio	1	212	212	80.6	0.0029
Error	3	7.90	2.64		
Total	8	7500			

A)



B)

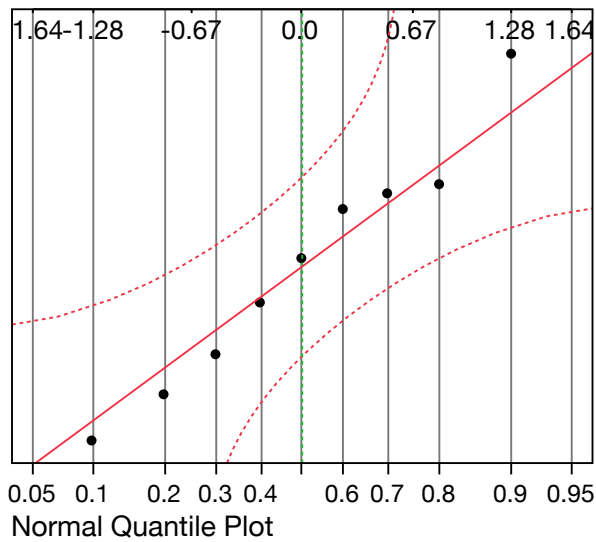


Figure S11. Residuals plots from response surface model of resin cracking (%). A) Residuals plots versus each explanatory variable and model prediction and B) Normal probability plot of residuals.

3.2 Resin Density Change

Differences in resin density were calculated following equation S11 to normalize resin addition in batch experiments. Results are presented in **Table S7**.

$$\text{mass NZVI A600E} * \frac{1 \text{ g A600E}}{1.13 \text{ g NZVI A600E}} = \text{density corrected mass NZVI A600E} \quad (\text{S11})$$

An example calculation is shown in equation S12. For a mass of 0.05 g NZVI-A600E used in a batch experiment, a density corrected mass of 0.044 g was used in isotherms to compare to unmodified A600E resin.

$$0.05 \text{ g NZVI A600E} * \frac{1 \text{ g A600E}}{1.13 \text{ g NZVI A600E}} = 0.044 \text{ g NZVI A600E (density corr.)} \quad (\text{S12})$$

Table S7. Resin mass change for 1 g of each resin in replicate.

Parameter	A600E	FeCl4--A600E	NZVI-A600E
Mass increase from A600E (air dried) (%)	-	26.21 ± 0.09	13 ± 2
Mass loss in oven (%)	8.8 ± 0.4	4.3 ± 0.1	7.9 ± 0.2

3.3 Batch Experiments

Figure S12 shows photos of bottles at each isotherm condition after 24 hours. The characteristic green-yellow color of chromate disappears from solution as solution volume decreases and more chromate exchanges onto the resin (**Figure S12A**). The grey-black color of the NZVI-A600E solutions may have come from the dark color of the iron (**Figure S12B**). However, no dissolved iron was detected in the batch experiments solutions, indicating that the dark color of the iron may have been in particulate form rather than dissolved.

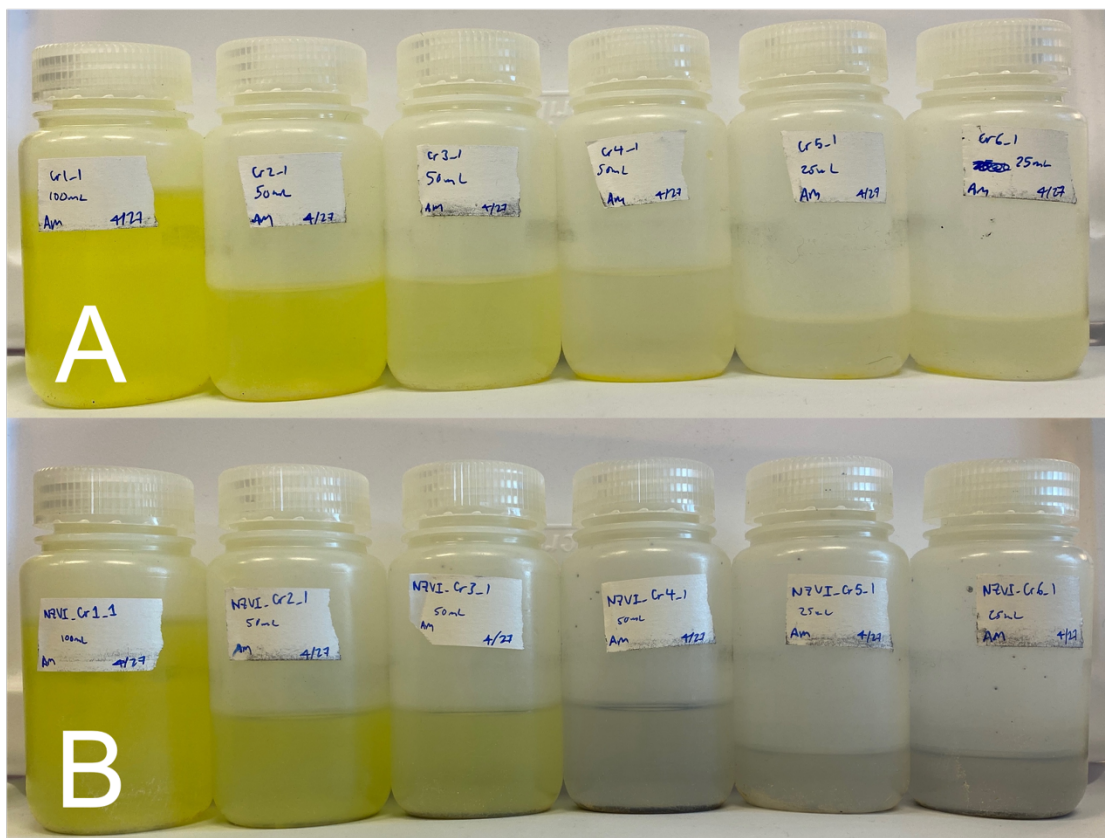


Figure S12. Photos of bottles for each isotherm condition after 24 hours for A) A600E and B) NZVI-A600E.

Different empirical isotherms were fit to the data during the loading of FeCl_4^- onto the resin. The Freundlich isotherm best represented the observed data as it is not constrained to plateau at a maximum concentration. The 95% joint confidence region between parameters showed a correlation between parameter estimates. The root mean square error (RMSE) was 4.9. A Langmuir isotherm was fit but it did not describe the data adequately as the solid-phase concentration never exhibited a plateau representative of a maximum capacity (**Figure S13C**). Best-fit parameter estimates are not reported because the model did not fit the data adequately. A three parameter Redlich-Peterson isotherm was fit. A solution that minimized sum-squared error was identified, but the model parameters were ill-conditioned. Two of the terms (K_{RP} and a_{RP}) had

a joint probability confidence region that showed strong correlations between parameter estimates and included zero.

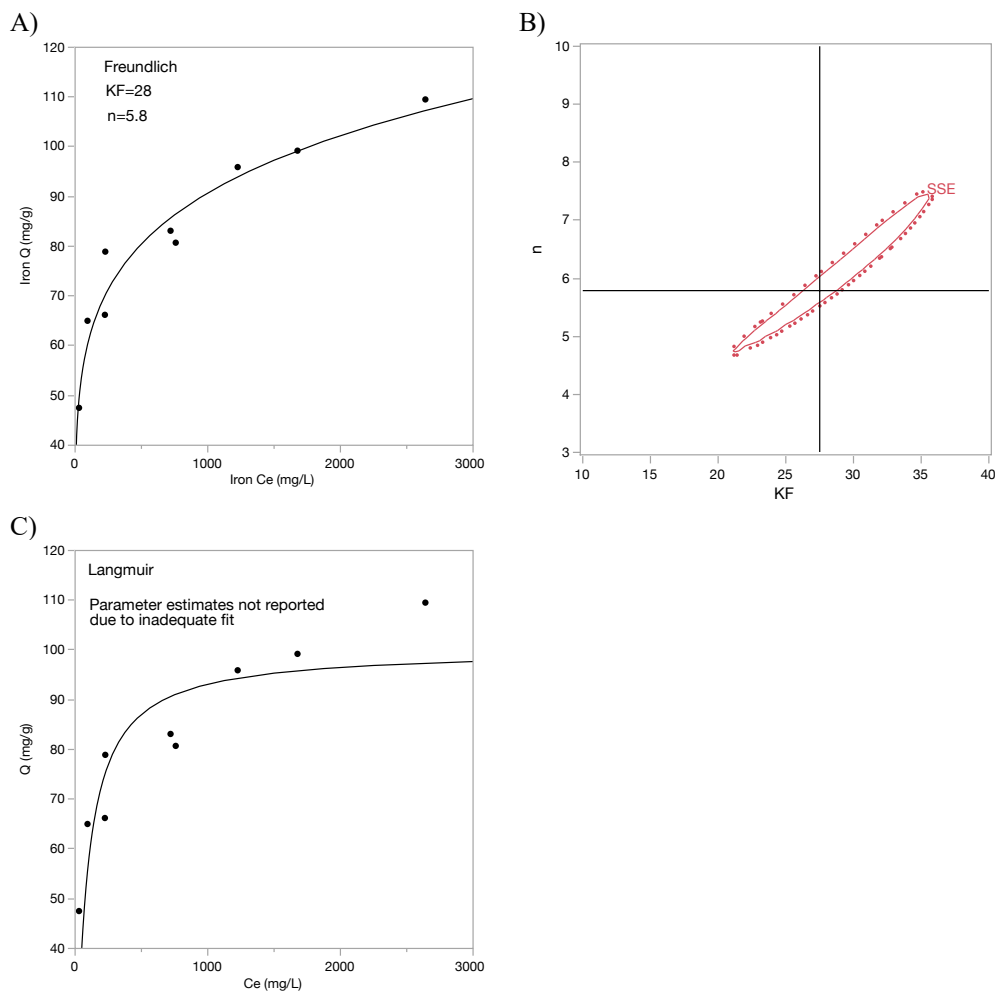


Figure S13. Isotherm models for FeCl_4^- loading onto A600E resin, where C_e (mg/L) is the concentration of iron in solution and Q (mg/g) is the mass of iron loaded onto the resin. A) The best-fit Freundlich model, B) The joint probability confidence regions for Freundlich parameter estimates, and C) The best-fit Langmuir model. The units of K_F are $\text{L}^{1/5.8} \text{mg}^{1-1/5.8} \text{g}^{-1}$

Table S8. Parameter estimates and 95% confidence limits (CL) for the Freundlich isotherm

Isotherm Model	Parameter	Units	Estimate	Approx. Std. Error	Lower CL	Upper CL
Freundlich	K_F	$\text{L}^{1/n} \text{mg}^{(1-1/n)} \text{g}^{-1}$	27.5	3.17	20.7	35.8
	n	—	5.79	0.57	4.66	7.52

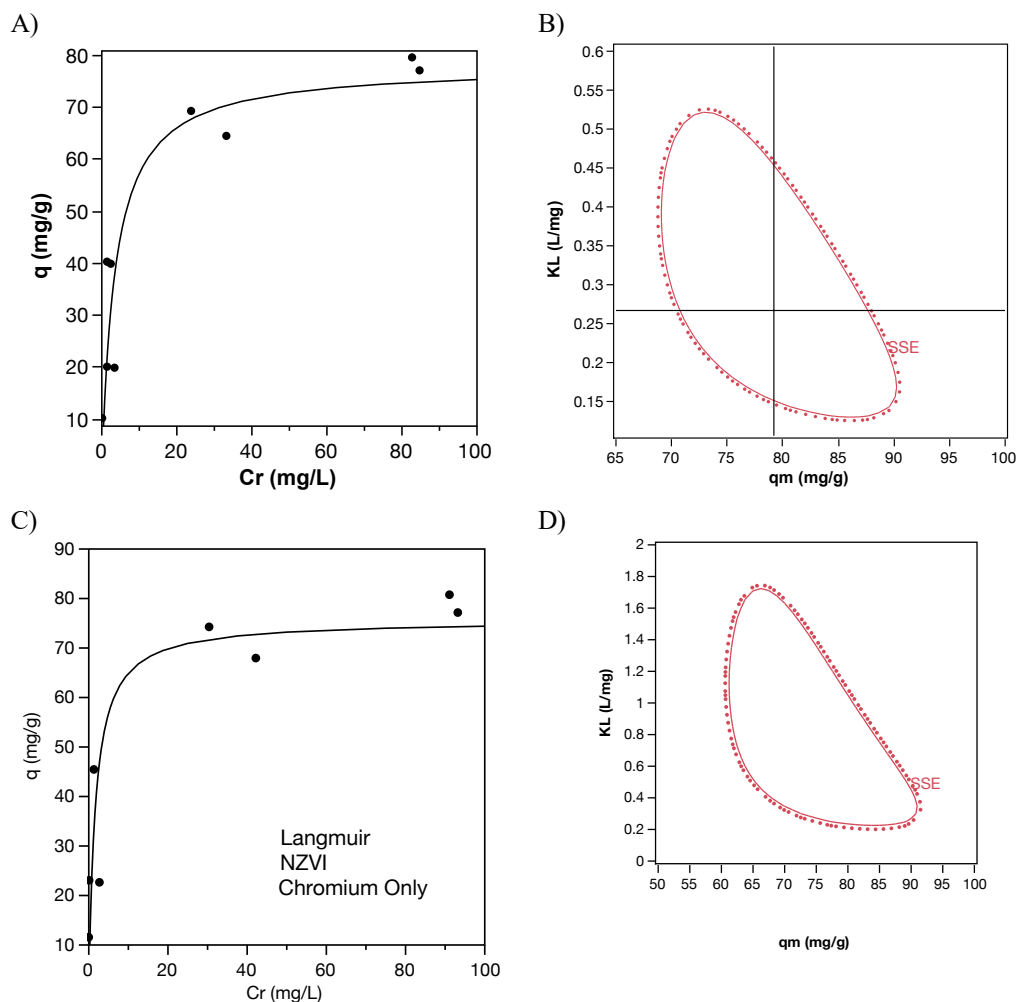


Figure S14. Langmuir isotherm models for Cr(VI) loading onto A600E resin (A-B) and NZVI resin (C-D) in a model solution containing only Cr(VI). A,C) The best-fit isotherm model and B,D) the joint probability confidence regions for isotherm parameter estimates.

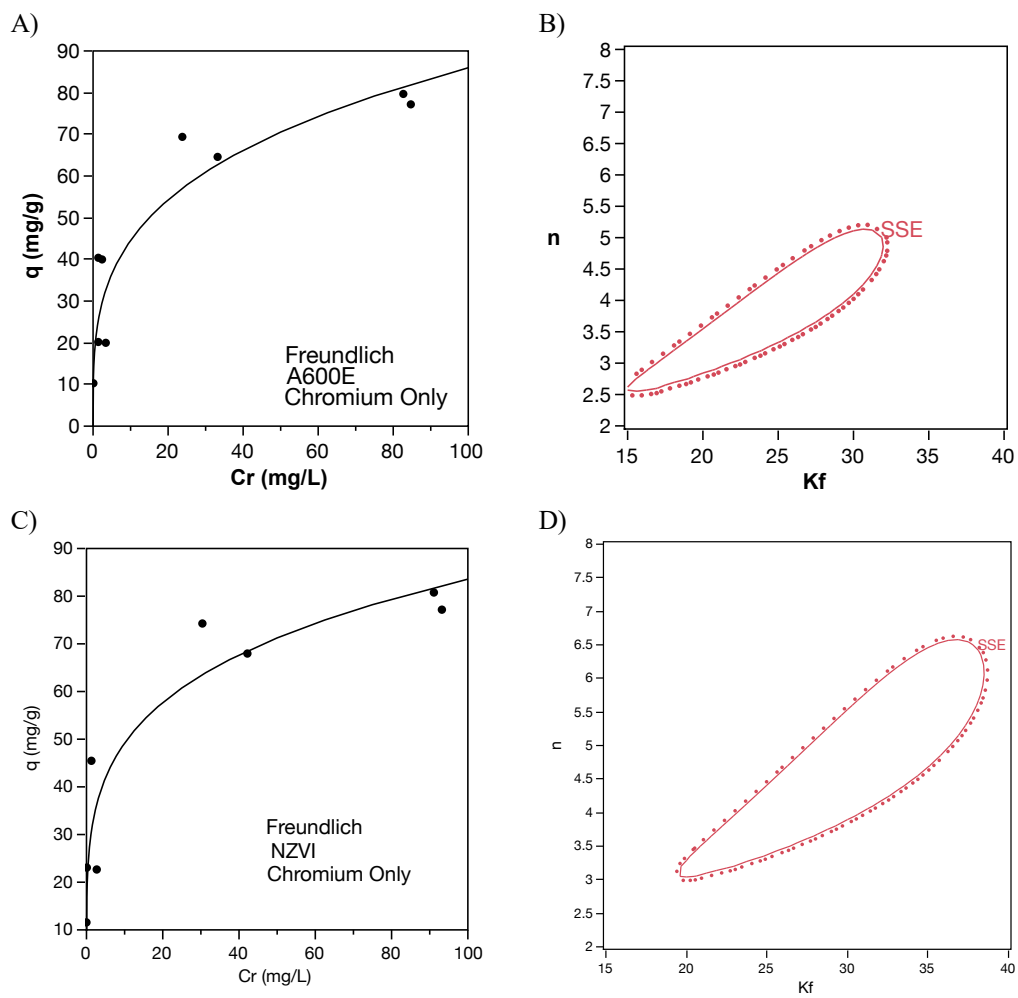


Figure S15. Freundlich isotherm models for Cr(VI) loading onto A600E resin (A-B) and NZVI resin (C-D) in a model solution containing only Cr(VI). A,C) The best-fit isotherm model and B,D) the joint probability confidence regions for isotherm parameter estimates. The units of K_F are $L^{1/n} \text{ mg}^{1-1/n} \text{ g}^{-1}$.

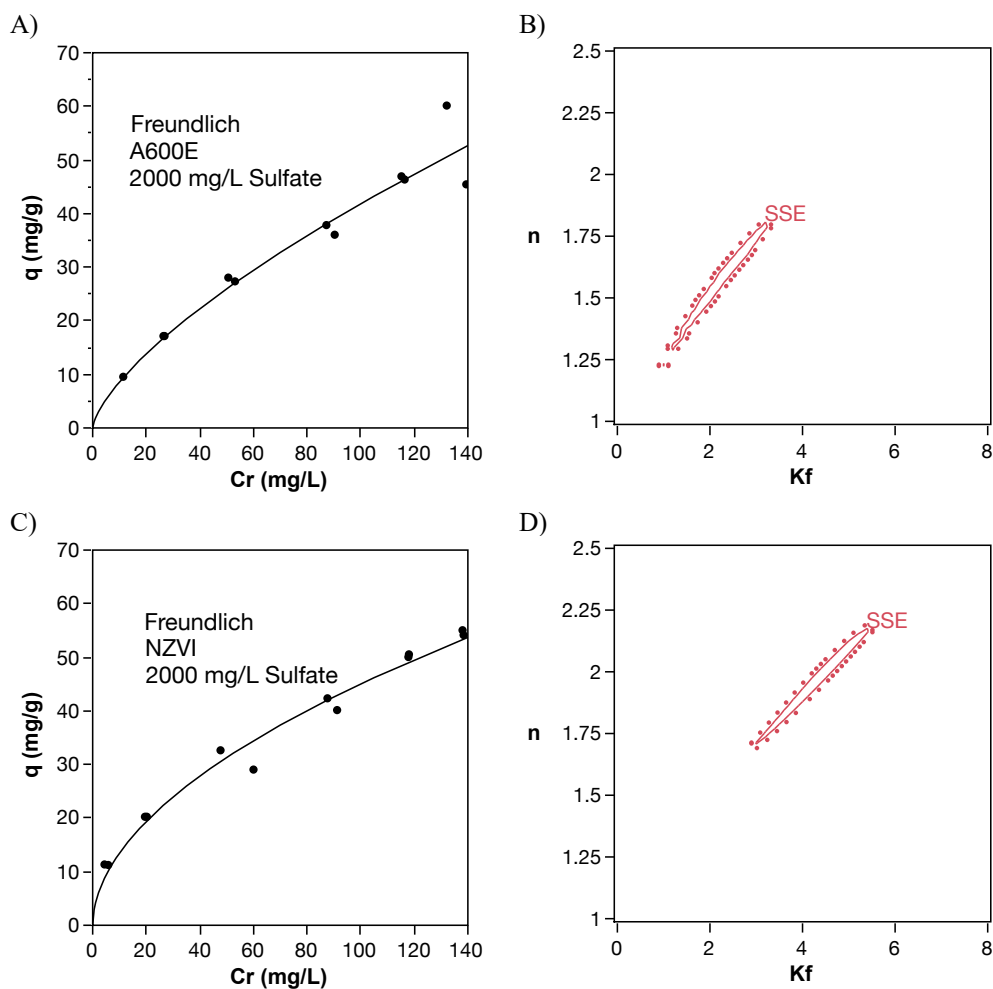


Figure S16. Isotherm models for Cr(VI) loading onto A600E resin (A-B) and NZVI resin (C-D) in a model solution containing Cr(VI) and 2000 mg/L sulfate. **A,C)** The best-fit isotherm model and **B,D)** the joint probability confidence regions for isotherm parameter estimates. The units of K_F are $L^{1/n} mg^{1-1/n} g^{-1}$.

Table S9. Parameter estimates and 95% confidence limits (CL) for isotherms describing chromium removal on resin

Matrix	Material	Isotherm	Parameter	Units	Estimate	Approx. Std. Error	Lower CL	Upper CL
Cr(VI) Only	A600E	Langmuir	q_m	mg/g	79.2	4.6	69.1	90.3
			K_L	L/mg	0.3	0.08	0.13	0.52
	NZVI (Density corrected)	Langmuir	q_m	mg/g	75.6	6.16	61.2	100.0
			K_L	L/mg	0.60	0.22	0.22	1.72
2000 mg/L SO ₄ ²⁻	A600E	Freundlich	K_F	L ^{1/n} mg ^(1-1/n) g ⁻¹	1.77	0.58	0.80	3.44
			n	–	1.46	0.15	1.17	1.85
	NZVI (Density corrected)	Freundlich	K_F	L ^{1/n} mg ^(1-1/n) g ⁻¹	4.03	0.61	2.79	5.58
			n	–	1.91	0.12	1.66	2.21

3.4 Fluidized Bed Calculations

While the NZVI-A600E resin outperformed the A600E in the column experiment for selective Cr(VI) removal, there were a number of factors to take into account that would have practical implications for full-scale processes. First, since both columns were run upflow, despite using the same wet volume of resin, volumetric flow rate, and column, the heavier NZVI-A600E had a smaller expanded bed height than the A600E. There was an 21% difference in bed height between the resins, as listed in **Table S10**, with A600E resin expanding more due its lower density.

Table S10. Expanded heights of A600E and NZVI-A600E in upflow column experiments.

Resin	Expanded Bed Height (inch)
A600E	13
NZVI-A600E	11.25

To account for this difference in resin density, which may have biased the data in favor of NZVI-A600E performance, the following calculations were performed, shown in **Table S11**.

Table S11. Experimental parameters for fluidized bed experiments.

Parameter	A600E	NZVI-A600E
Fixed bed height (m)	0.217	0.217
Expanded bed height (m)	0.330	0.286
Fixed bed resin porosity	0.375	0.326
Expanded bed resin porosity	0.588	0.524
Bed expansion (%)	52	31

Fixed bed resin porosity for both A600E and NZVI-A600E resin were estimated to be 0.375 based on medium (0.30-0.80 mm) spherical particles²⁶. Expanded bed resin porosity was calculated according to equation S13²⁷:

$$\frac{L_{Expanded}}{L_{Fixed}} = \frac{1 - \varepsilon_{Fixed}}{1 - \varepsilon_{Expanded}} \quad (S13)$$

where L is bed height in meters and ε is bed porosity, which is dimensionless. Thus, expanded bed porosities for each material are calculated in equations S14-S15:

$$\begin{aligned} \varepsilon_{Expanded,A600E} &= 1 - \left[(1 - \varepsilon_{Fixed,A600E}) * \frac{L_{Fixed,A600E}}{L_{Expanded,A600E}} \right] \\ &= 1 - \left[(1 - 0.375) * \frac{0.217}{0.330} \right] = 0.588 \end{aligned} \quad (S14)$$

$$\begin{aligned} \varepsilon_{Expanded,NZVI-A600E} &= 1 - \left[(1 - \varepsilon_{Fixed,NZVI-A600E}) * \frac{L_{Fixed,NZVI-A600E}}{L_{Expanded,NZVI-A600E}} \right] \\ &= 1 - \left[(1 - 0.375) * \frac{0.217}{0.286} \right] = 0.524 \end{aligned} \quad (S15)$$

Since the expanded bed porosities between A600E and NZVI-A600E were similar (0.588 compared to 0.524), the resin density difference likely had minimal biased on breakthrough. However, to remove the uncertainty due to differences in porosity between NZVI-A600E and A600E, a packed bed column experiment would be a better way to compare breakthrough for future experiments.

3.5 Post-Column Characterization

After column experimentation, the four cross-sections of the column were examined with the dissecting microscope as shown in **Figure S17**. The resin at the very top of the column, denoted as finer particulates, was bright orange and appeared to be broken pieces of resin that had risen to the top of the column. The top, middle, and bottom section of resin were also no longer black but a reddish-orange-brown color. This indicates that the Fe^0 was oxidized over the course of the experiment. **Figure S18** documents the XPS full scan for A600E, NZVI-A600E and post-column NZVI-A600E.

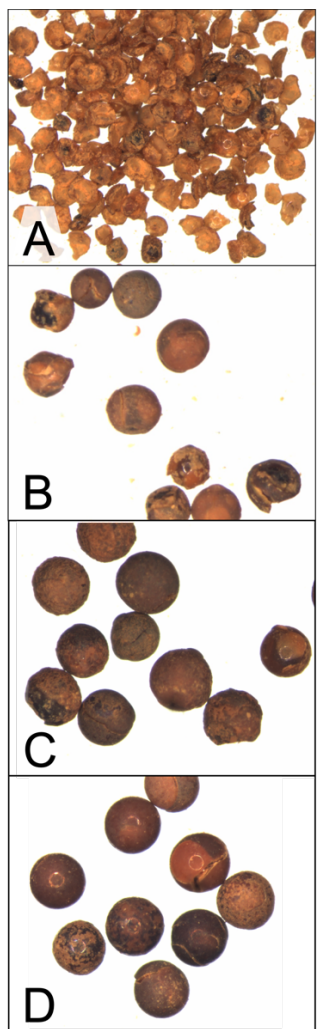


Figure S17. Images of post-column NZVI-A600E (A) finer particulates (B) top, (C) middle, and (D) bottom sections.

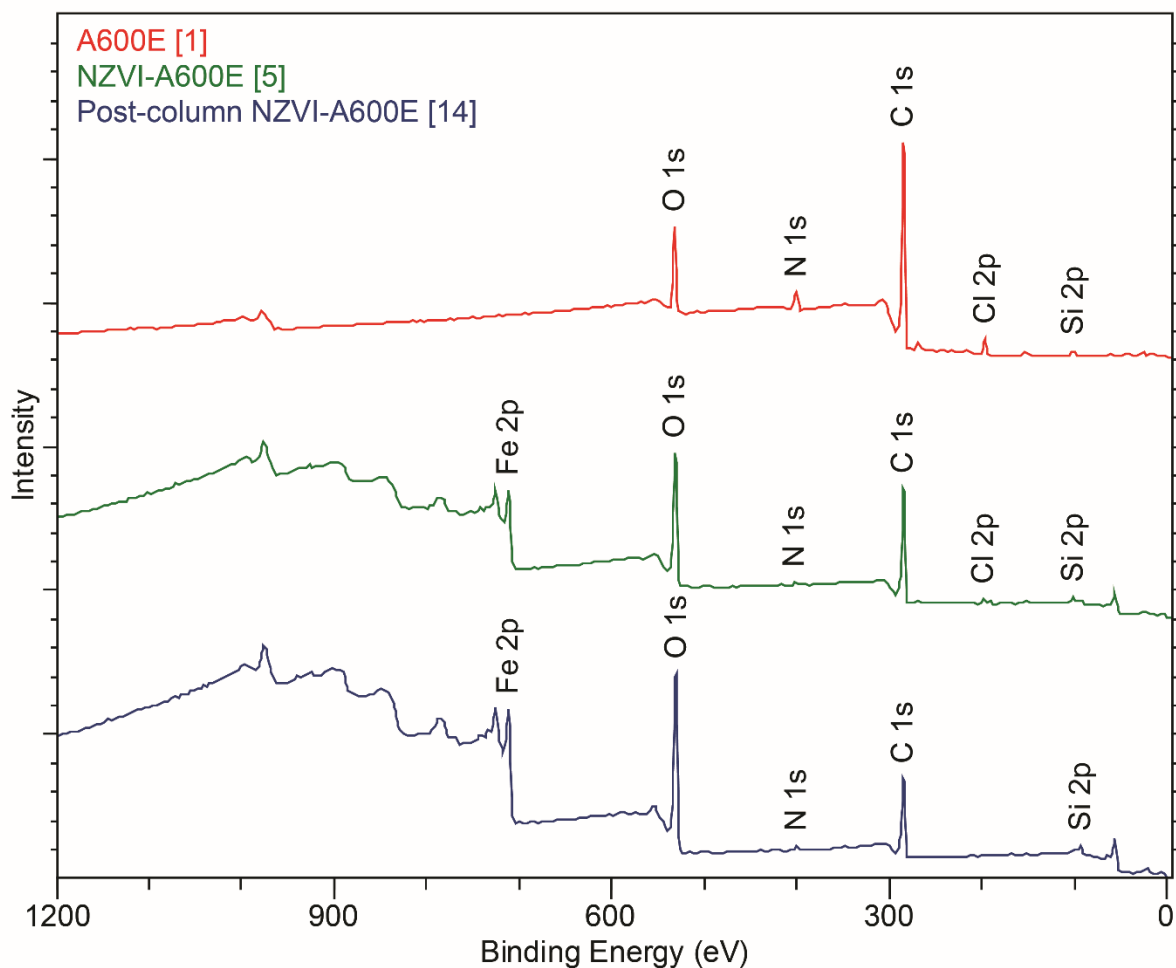


Figure S18. XPS spectrum of A600E, NZVI-A600E, and post-column NZVI-A600E.

4 References

- 1 R. Saha, R. Nandi and B. Saha, *Journal of Coordination Chemistry*, 2011, **64**, 1782–1806.
- 2 M. Bryjak, N. Kabay, B. L. Rivas and J. Bundschuh, Eds., in *Innovative Materials and Methods for Water Treatment*, CRC Press, 353–388.
- 3 S. E. Fendorf, *Geoderma*, 1995, **67**, 55–71.
- 4 M. M. Benjamin and D. F. Lawler, *Water Quality Engineering: Physical / Chemical Treatment Processes*, John Wiley & Sons, 2013.
- 5 L. M. Haupert, J. G. Pressman, T. F. Speth and D. G. Wahman, *AWWA Water Science*, , DOI:10.1002/aws2.1222.

- 6 F. Fu, J. Ma, L. Xie, B. Tang, W. Han and S. Lin, *Journal of Environmental Management*, 2013, **128**, 822–827.
- 7 A. Toli, K. Chalastara, C. Mystrioti, A. Xenidis and N. Papassiopi, *Environmental Pollution*, 2016, **214**, 419–429.
- 8 W. Gao, D. Zhong, Y. Xu, H. Luo and S. Zeng, *Journal of Dispersion Science and Technology*, 2022, **43**, 1197–1207.
- 9 A. Toli, Ch. Mystrioti, A. Xenidis and N. Papassiopi, *Bull Environ Contam Toxicol*, 2021, **106**, 409–414.
- 10 A. Toli, C. Mystrioti, I. Avgoustidis and N. Papassiopi, *Chemosphere*, 2021, **279**, 130472.
- 11 Z. Jiang, L. Lv, W. Zhang, Q. Du, B. Pan, L. Yang and Q. Zhang, *Water Research*, 2011, **45**, 2191–2198.
- 12 Y. Nomura, D. Inoue and Y. Moritomo, *RSC Adv.*, 2022, **12**, 17932–17936.
- 13 A. K. SenGupta, *Ion Exchange in Environmental Processes: Fundamentals, Applications and Sustainable Technology*, Wiley, 2017.
- 14 United States, US9138737B2, 2015.
- 15 G. Liu, C. Han, M. Kong, W. H. M. Abdelraheem, M. N. Nadagouda and D. D. Dionysiou, *ACS EST Eng.*, 2022, **2**, 1454–1464.
- 16 Y. Song, Y. Zeng, T. Jiang, J. Chen and Q. Du, *Nanomaterials*, 2022, **13**, 116.
- 17 C. Tai, J. She, Y. Yin, T. Zhao and L. Wu, *J nanosci nanotechnol*, 2016, **16**, 5850–5855.
- 18 Z. Jiang, S. Zhang, B. Pan, W. Wang, X. Wang, L. Lv, W. Zhang and Q. Zhang, *Journal of Hazardous Materials*, 2012, **233–234**, 1–6.
- 19 Y. Song, Y. Zeng, J. Liao, J. Chen and Q. Du, *Chemosphere*, 2021, **269**, 128684.
- 20 L. C. Flint, M. S. Arias-Paić and J. A. Korak, *Environ. Sci.: Water Res. Technol.*, 2021, **7**, 2397–2413.
- 21 C. Gorman, C. Seidel, T. Henrie, L. Huang and T. Robert, *jawwa*, 2016, **108**, E240–E246.
- 22 Purolite, Purolite Product, <http://www.purolite.com/product/a500plus>, (accessed July 5, 2023).
- 23 A. Lace, D. Ryan, M. Bowkett and J. Cleary, *IJERPH*, 2019, **16**, 1803.
- 24 G. W. Haupt, *Journal of Research of the National Bureau of Standards*.
- 25 M. S. Arias-Paić and J. A. Korak, *Environ. Sci. Technol. Lett.*, 2020, **7**, 111–117.
- 26 N. Ouchiyaama and T. Tanaka, *Ind. Eng. Chem. Fund.*, 1984, **23**, 490–493.

- 27 J. C. Crittenden, R. R. Trussell, D. W. Hand, K. J. Howe and G. Tchobanoglous, *MWH's Water Treatment: Principles and Design*, John Wiley & Sons, 2012.